Low latitude Tethyan calcareous nannofossil ocean paleoecology across the early/middle Eocene transition

M. Weinbaum Hefetz[1], O. M. Bialik[2] and C. Benjamini[1]

[1] Department of Earth and Environmental Sciences, Ben-Gurion University in the Negev, Be'er Sheva 84105, Israel

[2] The Dr. Moses Strauss Department of Marine Geosciences, Charney School of Marine Sciences, University of Haifa, Mount Carmel, 31905 Haifa, Israel

Corresponding author: Menahem Weinbaum Hefetz (hefetzwe@post.bgu.ac.il); Or M. Bialik (oblialik@staff.haifa.ac.il)

Key Points:

- The southern Tethyan remained stratified long after global mixing has begun in the ocean, due to the effect of proximity to the shelves of the Afro-Arabian margin.
- The southern Tethys differed from other oceanic sites as the general trend interrupted by short-term events from cooler boreotropical sources.
- By taking surrounding hinterland input under consideration, studies of land-enclosed seas augment understanding of global paleoceanographic factors.

Plain Language Summary

A major ecological reorganization of calcareous nannoplankton populations took place in the Eocene, in response to one of the largest global warming events in earth history (Early Eocene Climate Optimum, EECO), and its cool aftermath. These events were explored mainly in open ocean sites. We compare here the Tethyan pelagic record from Avdat, southern Israel, to Deep Sea and Ocean Drilling sites. The Avdat calcareous nannoplankton assemblages comply with global trends but acmes of cooling markers (e.g. genus *Reticulofenestra*) were delayed by ~1.0 Myr at Avdat. Notably, trends at Avdat are uniquely interrupted by short-term events that express rapid, temporary occurrences of nutrient input or water mixing markers. The southern Tethyan marginal ocean remained stratified although global mixing had begun in the open ocean, that can be attributed to warm climate and proximity to saline shelves of the Afro-Arabian continent. Likewise, interruptions in the record are a consequence of the unique contributors of water in the

Levant basin, at times from the warm, arid Afro-Arabian Tethyan margin to the south, but increasingly from cooler waters sourced in the boreo-tropical ocean.

Keywords:

Calcareous nannofossil, Pelagic paleoecology, Levant margin, Delayed destratification, *Reticulofenestra* acme

Abstract

Calcareous nannoplankton population underwent a major reorganization across the early and middle Eocene. This reorganization was mainly explored from an open ocean perspective, but marginal settings are usually underexplored. Here we analyzed a Tethyan pelagic record from Avdat, southern Israel in the Levant margin. The calcareous nannofossil assembledge was then compared to a number of Deep Sea and Ocean Drilling sites through paleoecological techniques. From calcareous nannofossil zone NP12 until zone NP15-16 (undiff.), dominance shifted from *Toweius* to discoasters in the warm early Eocene, and then to *Reticulofenestra,* responding to cooling in the middle Eocene. Markers for middle Eocene oceanic destratification and mixing, e.g., the *Reticulofenestra* acme, *Chiasmolithus* peak and the first occurrence of *Cyclicargolithus luminis*, are delayed by ~1.0 Myr at Avdat with respect to oceanic sites at comparable paleolatitudes, and more so when compared to higher latitude sites. The Avdat section is punctuated by peaks of *Thoracosphaera*, diversity of *Blackites* spp., and *Braarudosphaera,* that were not reported in deep oceanic sites. The disparities at Avdat vs. other oceanic localities can be ascribed to its position in a Tethyan remnant ocean surrounded by land masses and orogenic terrains. The punctuational mode and delay in water destratification in the Levant ocean are attributed to connection to warm and saline water off the Afro-Arabian shelf affected by pulses of cooler waters from Boreotropical marine connections, and sea level fall late in the Middle Eocene, increasing proximity to shelves.

1. Introduction

Over the last two decades, quantitative paleoecological approaches have increasingly been applied to Paleogene calcareous nannofossil assemblages. Several groups of calcareous

nannofossils were found to be good markers for changes in Paleogene palaeoceanographic conditions (Bralower, 2002; Tremolada & Bralower, 2004). The discovery of the discoaster acme marking the Early Eocene Climate Optimum (EECO, 49.4 - 53.3 Ma) by Aubry (1986), was later quantitatively described by Agnini et al. (2006). Assemblages dominated by *Chiasmolithus* spp. were used as proxies for high trophic conditions, elevated nutrients and cooler waters (Tremolada & Bralower, 2004). Schneider et al (2011) described latitudinal influence on calcareous nannofossil assemblages, as well as the major role played by the Oceanic Biological Pump (OBP) in temperate climate zones (see Hilting et al., 2008). Tori and Monechi (2013) quantified the important re-organization of calcareous nannofossil assemblages during the Ypresian/Lutetion transition, when *Reticulofenestra* replaced *Toweius* and *Discoaster* spp. as the dominant group in middle Eocene assemblages. Calcareous nannofossil assemblage data augmented by stable isotopes tracked the warm oligotrophic conditions that prevailed during the Paleocene-Eocene Thermal Maximum (PETM) and subsequently during the EECO. Galeotti et al. (2019) found several carbon isotope excursions (CIE's) paced by orbital forcing at the early/middle Eocene transition.

Most of these palaeoceanographic studies concentrated on tracking the global ocean using cores recovered by the Deep-Sea Drilling Project (DSDP) and Ocean Drilling Project (ODP) in the Atlantic and Pacific, while paleoecological data from Tethyan land-based localities tend to be under-represented. Knowledge gaps have developed regarding the way marginal or epicontinental, and in general lower latitude small oceanic basins reacted to the course of events across the early/middle Eocene transition. However, the eastern Mediterranean persisted as an important gateway between the Neo-Tethyan-Indian-Pacific, the Mediterranean Tethyan remnant and the Atlantic oceans. The current study is a reevaluation of the paleoceanography of the well-represented onshore Eocene pelagic record of the eastern Mediterranean Levant region, by comparison of calcareous nannofossil assemblages under a subtropical climate regime, surrounded by the Arabian plate and tectonic landmasses, in order to explain departures from global trends in this small but critical oceanic realm.

1.1 Geological settings

The Levant region represents the distal limit of the northwestern carbonate-dominated ramp of the African -Arabian platform in the Late Mesozoic – Early Cenozoic, located in the zone

of transition from the tropical to subtropical climate bands (Fig. 1). During the Paleogene, The Levant margin (Fig. 2) was blanketed by extensive hemipelagic to pelagic marl and chalk deposits (Speijer, 1995; Dercourt et al, 1993; Scheibner & Speijer, 2008).

Speijer (1995) observed a continuous northward increase in water depth in Egypt from shoreface to bathyal in the Paleocene of the Levant basin margin. This ramp descended from the shoreline near the Sudanese border to more than 500 m depth in the northern Nile valley outcrops. To the northeast, most of Sinai and southern Israel were more distal and presumed to be at bathyal depths (Speijer, 1995). Schmitz et al. (1997) used barium, silica and phosphorous proxies to reconstruct biological productivity from the Paleocene to the Eocene, that indicated a trophic perturbation in line with the abrupt change in southern Tethyan upwelling at the P/E boundary (Gangyi et al., 1995). Scheibner and Speijer (2009) later attributed changes in Paleogene oceanic faunal assemblages in Egypt to sea surface temperature, oceanic acidification and trophic level perturbations. In contrast, Aubry and Salem (2013), using calcareous nannofossil assemblages, suggested that the biota was responding to differential rates of Paleocene - Early Eocene subsidence following intense regional tectonic activity in the middle to late Paleocene.

Among the best described outcrops of the Paleocene and Eocene in this region are those of the Zin Valley and the adjacent Avdat plateau in southern Israel, mapped by Avni and Weiler (2013). The lithology of the Lower Eocene part is bedded white or grey chalk with bands of chert nodules (Fig. 3) of the Mor Formation The chalk is composed nearly entirely of biogenic carbonate, more than 85% of calcareous nannofossils, and the remainder mostly planktonic foraminifera and few benthic, with high P/B ratio (Benjamini, 1979, 1980; Fermont, 1982). Diatoms, radiolarians and siliceous sponge spicules were also reported in Eocene chalks (Braun, 1967; Ehrlich & Moshkovitz 1982) and are the source of silica for the chert interbeds. The Lower Eocene chalk may contain as much as 5% euhedral dolomite rhombs to a few tens of microns in length (Braun, 1967). Chalk beds are interrupted by burrowed horizons, predominantly by *Thalassinoides*, that may be partially or completely filled with, or replaced by, dark, zoned chert. Occasional interbeds of brown organic-rich chalk, to 20-50 cm in thickness, are also present. Organic-rich chalk horizons with measured total Organic Carbon (TOC) of up to 2-3% are of regional importance and potentially commercial deposits were described in the north of Israel (Weinbaum- Hefetz & Bartov, 2019; Bartov et al, 2019; Meilijson et al, 2019, mostly commercial data), as well as in the NP13-NP15 interval in Jordan (Alqudah et al, 2015). These occurrences are

a temporal continuation of the Late Cretaceous organic-rich chalk lithofacies localized in structural depressions that is commercially exploited as oil shale. (Ashckenazi-Polivoda, 2011; Meilijson et al., 2014). Within the middle Eocene, the pelagic chalk becomes more homogeneous and frequency of chert horizons falls sharply (Horsha Fm). In the middle Eocene, sporadic horizons with winnowed grains of glauconite occur, often as foraminiferal test infillings.

Two intervals with indurated wackestone lithofacies containing transported larger foraminifera, interbedded with the autochthonous pelagic chalks, are prominent in Avdat sections. The two intervals occur at the boundary with the Middle Eocene, mapped as the Nizzana Fm, and within the Middle Eocene, mapped as the Matred Fm (Braun, 1967; Benjamini 1979, 1980; Fermont 1982; Weinbaum-Hefetz & Benjamini, 2011). These are mass-transport deposits (MTD's, see Fig. 3) in which the larger foraminiferal lithofacies is emplaced into the depositional environment of autochthonous pelagic chalk sediment. Detachment, transport and emplacement with associated deformation features has been described from within the pelagic lithofacies as well (Buchbinder et al., 1988). The regional paleobathymetric framework was interpreted as a homoclinal carbonate ramp that became distally steepened in the middle Eocene.

1.2 Biostratigraphy

Earlier studies on the biostratigraphy of the Avdat region concentrated on planktic foraminifera (Benjamini, 1980; Benjamini, 1995). The first study on the calcareous nannofossil biostratigraphy at Avdat was carried out on the Paleocene and lower Eocene by Romein (1979). Moshkovitz (1995) together with Schaub (1995) and Benjamini (1995) published an integrated correlation using calcareous nannofossils, nummulites and planktic foraminifera (Schaub et al., 1995). An updated biostratigraphy based on calcareous nannofossils correlated to an updated age-model was by Weinbaum-Hefetz and Benjamini (2011). The succession begins at NP11 (biostratigraphic schemes of Martini, 1971, and Okada & Bukry, 1980), and terminates in the undifferentiated NP15-16 (Fig. 3). Preservation of the calcareous nannofossils is generally good, with ca. 100 species identified (Romein, 1979; Moshkovitz, 1995). Rates of sedimentation increased from ~6 m Myr^{-1} in the early Eocene to ~40 m Myr^{-1} in calcareous nannofossil zone NP14 (Fig. 3e) and declined to 11 m Myr^{-1} in NP15-16 (undif.). Some typical Paleocene calcareous nannofossil species (*Ellipsolithus macellus*, several *Cruciplacolithus* spp.) were apparently reworked into the section, especially around the NP14/15 transition (Weinbaum-Hefetz &

Benjamini, 2011). Alqudah et al. (2015) also reported on several reworking peaks in Jordan, attributing them to contemporaneous tectonic activity.

5. Methods

In the current study, samples studied by Weinbaum Hefetz and Benjamini (2011) were recounted and the data was reprocessed. The 200 samples were originally taken from seven subsections (Fig 2: EA1-4, BR1-2, EL) along the Zin Valley ('Nahal Avdat' of Romein, 1979). The age-model of Weinbaum Hefetz and Benjamini (2011) was corrected according to the GTS 2012 (Schmitz, 2012) and the early / middle Eocene boundary was placed at the Ypresian / Lutetian transition marked as the NP14a / NP14b calcareous nannofossil biozone boundary (47.80 Myr). The error for the corrected age model is ±0.1 Myr.

2.1 Counting and statistical analysis methods

The counting procedure was based on the total number of specimens per View Field (pVF) following a uniform protocol. Rarefaction curves (SHE, Buzas & Hayek, 1998) reached count stability in 60 view fields per sample, taken from 5-10 slide replicates. Number of species was calculated together with the Simpson's Index of Dominance (Somerfield, 2008) ranging from 0 (all taxa are equally present) to 1 (one taxon completely dominates the assemblage). The nature of the data is non-parametric and all biotic counts were normalized by square root, and environmental data was log-normalized. In all statistical analyses, samples were coded by NP zones (11, 12, 13, 14, 15). Genera comprising less than 2% of the assemblage were disregarded to reduce stress analysis. In order to avoid predetermined assumptions, a Non-metric Multi-Dimensional Scaling projection (NMDS, 'ENVFIT') accompanied by a permutation test was used. Stress values of less than 10 were considered acceptable (Clarke, 1993; Clarke & Ainsworth, 1993). For comparison with ocean drilling sites, both NMDS and Detrended Correspondence Analysis (DCA) were used. A 2-way ANOSIM test was carried out on a rank matrix of the ocean drilling/Avdat sites. All statistical procedures were carried out using a Bray Curtis distance matrix with R-Statistics code of package Vegan 2.2-1.

2.2 Taxonomy

The current study generally follows systematics and nomenclature of Perch-Nielsen (1986), Young and Bown (1997), and Young et al. (1997) and uses the 103 taxa of Weinbaum -

Hefetz and Benjamini (2011). As biotic / environmental fitting procedure optimally works with as few variables as possible, the current study re-grouped the database with nine groups accounting for 70% of the total variance. These groups are: *Zygodiscales* Young and Bown 1997 (including helicospheres, pontospheres, scyphospheres and *Transversopontis* sp.); *Blackites* Hay and Towe 1962; *Reticulofenestra* Hay, Mohler and Wade 1966; *Chiasmolithus* Hay, 1966; *Coccolithus* Schwartz 1894 Young and Bown 1997; *Braarudosphaeraceae* Deflandre 1947, *Discoasteraceae* Tan 1927, Family *Sphenolithaceae* Deflandre 1952, and *Thoracosphaera* Kamptner 1927.

Some changes in taxonomical definitions required adjustment of groupings to enable comparison with other studies. Within the Family *Coccolithaceae* Poche 1913, Young and Bown (1997) placed all rimmed and open central area coccolithus –type placoliths into the modified taxon Coccolithus (*Coccolithus* Schwartz 1894, emend. Young & Bown 1997), while *Ericsonia* Black 1964 had been distinguished by other workers (e.g. Agnini et al, 2006; Schneider, 2011). The current study therefore referred only to *Coccolithus sensu stricto*. *Zygodiscales* was significant in the Avdat data and used for the ENVFIT projection but omitted from the Avdat vs. DSDP/ODP comparison due to insufficient data.

2.3 Environmental and biotic database

Numerical and graphical global oxygen and carbon stable isotope values were taken from the benthic foraminifera global database of Zachos et al. (2001; 2008). The Arabian Plate sea level record is from Haq and Al-Qahtani (2005). The global strontium isotope curve was taken from McArthur et al. (2001). The calcareous nannofossil counts in the Avdat assemblage are local biotic trends correlated to DSDP and ODP data from several oceanic sites (Schneider et al, 2011, repository data). The selected sites for comparison for tropical/subtropical latitudes were ODP Site 1210, North Pacific Shatsky rise and ODP Site 1263 for South Atlantic Walvis Ridge. For temperate latitudes, ODP Site 762 on the Indian Ocean Exmouth Plateau and DSDP Site 549 on the North Atlantic Goban Spur were chosen, representing the subtropical/boreal belt. The high latitude sites studied by Schneider et al (2011) were poorly comparable, as the common species are different. The current study correlated the published calcareous nannofossil biozones to the Martini (1971) biostratigraphic scheme, using only those samples from the NP12 to NP15-16 (undif.) that could be projected onto the age-model.

6. Results

Calcareous nannofossil counts from the integrated section of Avdat are presented in Fig. 4. The trend begins with *Toweius*, *Coccolithus*, discoasters and *Tribrachiatus orthostylus* dominant in the early Eocene (segment I), followed by rise in *Coccolithus* (segment II). Zygodiscales (pontospherids and helicospherids) and *Blackites* are found in the lower part of the middle Eocene and up to the NP14\15 boundary (segments III and IV). Above this point *Chiasmolithus* increases, to a point that *Chiasmolithus*, *Coccolithus* and *Reticulofenestra* are subequal (segments V and VI). The continued notable rise of *Chiasmolithus* (segment VII) is followed by a sharp fall of *Coccolithus* and an acme of sphenoliths in segment VIII in the upper part of the section (EL section, NP15-16 undif., segment IX), while the section terminates at the further rise of *Chiasmolithus* to dominance (segment IX).

R. dictyoda (Fig. 5b, 1-5%) occurs in small amounts early on and is present in most of the section. Just above NP14b (BR2-1, 46.2 Myr), *Reticulofenestra* spp. counts increase to around 20%, and then again to 60% in NP15-16 (undif.) (segment IX sample EL-25). Prior to this latter rise of *Reticulofenestra* sp., a sharp increase in sphenoliths is observed in segment VIII, just beneath the first occurrence of *R. umbilicus* (Fig. 5d). After this horizon, the age-model cannot be calculated but *Reticulofenestra* sp. counts reach ca. 80%.

Several prominent short-term peaks punctuate the general trend are shown in Fig. 4. Transitional horizons are mostly expressed by acmes of groups that are rare through the rest of the column, including *Thoracosphaera* and *Braarudosphaera* (Figs. 5c and 5f), and by poor preservation. In NP11 some rapid fluctuations include peaks of *Sphenolithus* and *Toweius* spp., below the constrained portion of the age model. In NP12 within segment I are two peaks of discoasters, *Toweius* and *Reticulofenestra* spp. separated by a lengthy time interval; samples EA1-7 and EA1-10 are of ages 56.0 Myr and 53.1 Myr respectively. The next short-term peak again occurs at the I/II transition following a lengthy time interval, at EA4-1 to EA4-4, within NP14a at 49.0 Myr. The first occurrence of *Cyclicargolithus luminis* (Fig. 5a) in EA4-14 is at the top of segment II at the end of the early Eocene at NP14a\b.

Several peaks occur within the middle Eocene, the lowest at 2m below the peak of *Blackites* and the FO of *B. piriformis* (Fig. 5e) at the segment II/III transition (samples EA4-16 and 17, 47.9 Myr), characterized by high abundance and diversity of *Blackites* spp. Above, a peak

of *Coccolithus* sp. occurs at the transition of segments III/IV (EA4-28 to BR1-1, 46.7 Myr). At the segment IV/V transition within the lower part of NP15-16 (undif.) at 46.0 Myr there is an event of increased abundance in *Thoracosphaera*, *Braarudosphaera*, discoaster and *Toweius*. In the transitional segment of VI/VII (BR2-55 to EL-5, 43.2 to 42.5 Myr) there is an additional peak of *Thoracosphaera*.

7. Eco-environmental analysis

4.1 Species richness and dominance

The pattern of segments, transitions and peaks of the total assemblage are reflected also in the dominance curve. The richness of the assemblage was calculated as the simple number of species in each sample (Fig. 6). Species richness peaks at the NP14b/15 boundary and falls again at the top of the studied section, high in the NP15-16 (undif.) zone. The Simpson's index of dominance generally demonstrates a reciprocal pattern with two climaxes: at the early/middle Eocene boundary, where *Coccolithus* sp. dominates, and in the uppermost part of NP15-16 (undif.), where *Reticulofenestra* sp. dominates.

4.2 Assemblage response to global variables

The Avdat assemblage was calibrated against published databases of global benthic foraminifera oxygen and carbon stable isotopes and the Arabian Plate sea level record used the NMDS-ENVFIT projection (Fig 7). The overall 2D stress of 0.14 points to diminished significance of any additional planes. Early Eocene samples (NP12 and NP13) are neutral to NMDS 1 and exhibit negative values along NMDS2, but by NP14a,b, samples move towards positive on NMDS2, then arch towards NMDS 1, and by NP15-16 the samples align well with NMDS1 and become neutral to NMDS2. However, the NP14a,b samples are broadly spread out, and many tend toward negative in NMDS1 including some prominent outliers, most notably in the EA4 section and one, BR2-8, in NP15-16 (undif.).

Calcareous nannofossil group *Toweius* spp. plots in the lower negative quadrant, and the sequence of *Toweius* to discoasters plots mainly along the NMDS1 axis. The early Eocene samples approach the field of *Sphenolithus*. The NMDS1 axis shows the Discoaster – *Coccolithus* shifting to positive as the samples arch from NP14b to NP15-16 towards this axis. The NMDS1 ends at *Reticulofenestra* and then *Chiasmolithus* to the right on this axis. The few outliers are strongly

negative in NMDS1 and approach the *Thoracosphaera* field in the upper quadrant. Clearly, in the middle Eocene, NMDS2 influence is very weak for the full sample set, but appears to strongly affect the samples producing the outliers, particularly EA-24.

Samples are spread out in the early Eocene and tend to cluster more strongly in the middle Eocene. Three environmental vectors can partially explain the NMDS 2D space. NMDS1 broadly follows $\delta^{18}O$ (R^2=0.44, $P_{(>r)}$ =0.001) and is stronger in the middle Eocene samples. NMDS2 more weakly follows $\delta^{13}C$ (R^2=0.30, $P_{(>r)}$ =0.001). The sea-level-change vector weakly corresponds to $\delta^{18}O$ but is poorly reflected in the samples (R^2=0.08, $P_{(>r)}$ =0.018), and is not further analyzed here.

4.3 Comparison to oceanic sites

A normalized and ranked data matrix was processed using NMDS, that consisted of nine taxonomic groupings that account for at least 75% of the total variance, taken from the Avdat sections and four DSDP\ODP sites oceanic sites of the database of Schneider et al (2011) (Fig. 8). Overall 2D stress is 0.19. A general feature of the projection is that points tend to scatter in the early Eocene mostly in the lower left quadrant, and migrate in the middle Eocene towards the upper right.

Some commonalities observed are that the distribution of species is in agreement with the ENVFIT performed for the Avdat samples. The lower left quadrant represents assemblages rich in *Toweius*, representative of the early Eocene warm temperature conditions. The samples then trend towards the upper right quadrant characterized by *Reticulofenestra*- and *Chiasmolithus*- rich assemblages, but the trajectories for each site are somewhat different. DSDP Site 1210 and ODP Site 1263 proceed along discoaster-*Chiasmolithus*-*Reticulofenestra*; DSDP Site 549 move from *Toweius* to *Sphenolithus* to *Reticulofenestra*, while ODP Site 762 moves directly from *Coccolithus* to *Reticulofenestra*. The Avdat succession parallels the trends observed in the ocean basins but is significantly shifted towards the upper left quadrant, a shift that is governed by *Braarudosphaera*, *Blackites* and *Thoracosphaera*. The outliers EA4-(1-4) in fact represent extremes of this shift of the Avdat assemblage, concentrated in the NP13-NP15 interval.

The difference between Avdat and the oceanic sites was tested using the ANOSIM test. A two-way ANOSIM test was carried out with a Bray Curtis distance and samples were factored by age (the early\ middle Eocene factor is 5\6) and by Avdat vs other sites (1\2 respectively). The age

factor gave a correlation of $R_{(age)}$ = 0.40 (P=0.001) while the site factor gave $R_{(site)}$ = 0.67 (P=0.001). Thus, Avdat as a site is more significantly different from oceanic sites, than are the ages of the samples.

The Euclidean Centroids of the 2D scores were calculated for each site \ age cluster (Fig. 8) and arrows represent both distance and direction of shifts. Trends are subparallel for three localities – Avdat, DSDP Site 549 and ODP Site 1263, with the magnitude of the shift greatest for DSDP Site 549, intermediate for the Avdat site, and lesser for ODP Site 1263. ODP Sites 762 and 1210 show far less movement in the right-hand half of the projection, compared to the first three sites.

In order to decipher the changes that take place during the NP13-NP15 interval in the Avdat section, a Detrended Correspondence Analysis (DCA) was performed on the same Avdat/deep ocean data matrix. Axes DCA1 (Eigenvalue of 0.33) and DCA2 (Eigenvalue of 0.35) explain 68% of the variance, so Axes DCA3 and DCA4 were omitted. The general negative trend from *Coccolithus* to *Reticulofenestra* on the DCA is common for most of the deep ocean sites. Comparison of trends emphasize that (a) the early Eocene of Avdat was closer to DSDP Site 549 in terms of *Sphenolithus:* (b) samples of EA4 section at NP14a\b including the outliers are uniquely attracted towards the *Thoracosphaera* and *Blackites* taxa, whereas most of the Avdat, and all deep ocean samples, were on the global trend of discoaster – *Reticulofenestra*. The unique path of Avdat in occasionally shifting strongly through *Thoracosphaera* towards *Blackites* during NP14a,b, and then backtracking to the oceanic trend, is therefore demonstrated by this method as well.

8. Discussion

5.1. Assemblage transitions and environmental implications

The successional sequence of *Toweius* → discoasters → *Reticulofenestra* observed in the Avdat section (Fig. 7) and the other sites (Fig. 8) relates to two main trends. The first is the long-term cooling trend from the EECO peak to the middle Eocene and development of latitudinal differentiation in plankton communities (Haq et a., 1977). The second relates to the export of the organic matter from the sea surface. It appears that organic carbon export rises through the early Eocene until a maximum in NP14 and then declines. Similar trend was also obtained from geochemical records, notably the Thallium isotopes record (Nielsen et al., 2009).

329 The path followed by each of the localities differs somewhat according to abiotic
330 conditions, presumably water stratification and mixing, possible upwelling, terrestrial input, saline
331 bottom water, etc. All sites exhibit the general temporal assemblage-shift from *Toweius*, towards
332 assemblages of *Chiasmolithus* and *Reticulofenestra* reflecting ocean cooling. DSDP Site 549 and
333 in ODP Site 1263 are more similar (NMDS1, Fig. 8), well away from *Blackites* and
334 *Thoracosphaera*. The Avdat assemblage shows some similarity to the trend of DSDP Site 549,
335 with the exception of the final detour at Avdat towards *Chiasmolithus* rather than *Reticulofenestra*
336 (Fig. 8).

337 In Avdat, *Braarudosphaera*, *Blackites* and *Thoracosphaera* are of greater significance
338 than at any of the ocean sites. Several horizons in Avdat during NP14 are 'hijacked' away from the
339 oceanic route along the assemblage space (Fig. 8), towards where *Blackites sp*. flourish together
340 uniquely with *Zygodiscales* (Fig. 4). The assemblage eventually continues towards *Chiasmolithus*,
341 but this transition occurs only after the NP14b /15 boundary (Fig 9).

342 The departure from the common trajectory during NP14a at Avdat is driven by the high
343 organic matter flux (NMDS 2, Fig 7, and see Fig. 8). Although the orientation of migrating vectors
344 was parallel, the shift towards *Thracosphaera* followed the progressive order of Site 1263 - Site
345 549 - Avdat. Compared to those three sites, ODP Site 1210 shows only a minimal effect within
346 the entire interval of NP12-NP15/16 (undif). It should be noted that in both Avdat and near Site
347 549, there are some evidence for the influence of upwelling systems in the early Eocene (D'haenens
348 et al., 2012; Schmitz et al., 1997). Such upwelling would have farther modified nutrient state and
349 enhance organic matter export.

350 In the open ocean *Thoracosphaera* sp. is less important during the early/middle Eocene
351 transition. *Thoracosphaera* sp. are calcareous dinoflagellates distinct from coccolithophores in
352 their ecological role. Thoracosphaeres flourished also around the extinction event at the K/Pg
353 boundary (Eshet et al, 1992; Tantawy, 2003), as well as in the Messinian Salinity Crisis (e.g. Bison,
354 2007). Kohn and Zonneveld (2010) found that modern *T. heimii* is most abundant in well-mixed
355 waters of the upper photic zone, in upwelling systems or at episodes of high riverine influx of
356 nutrients. By extension, *Thoracosphaera* at Avdat represents a proxy for a rapid episode of nutrient
357 input or salinity change.

The *Blackites* group is more complex (Shafik, 1989) and their low diversity at most deep-sea sites precludes using them as proxies for paleoecological conditions. However, high diversity in Avdat was reported by Weinbaum-Hefetz et al. (2000) and Weinbaum Hefetz and Benjamini (2011). Seven taxa were described but the genus was difficult to cluster into definitive species. They suggested that morphological variety might represent a phenotypic response to physical parameters of sea water. A similar or even more diverse representation of this group was described from the Lodo Formation of California (Bramlette & Sullivan, 1961). Eleven taxa were described that mostly occurred around the FO of *B. inflatus* (*'Rhabdosphaera inflata'*). Ozdinova (2013) considered blooms of *Blackites* as proxies for short warming episodes, but our ENVFIT (Fig. 7) does not corroborate a temperature component.

5.2. Perspective on the Tethyan response in the Eocene

The biogeographic effects of the middle Eocene cooling are diachronous. The occurrence of the end-member assemblages (*Chiasmolithus* and *Reticulofenestra*) at Avdat and all other localities is a global commonality in the middle Eocene. Agnini et al. (2007) detected the earliest specimens of *Dictyococcites* at the NP12\NP13 transition (50.5 Ma). Schneider et al (2011) found the first occurrence (FO) of *Reticulofenestra dictyoda* at polar localities at ca. 52 Myr, but occurring later at temperate and tropical sites. *R. dictyoda* was found by Bown and Newsam (2017) in the North Atlantic in NP12 (53.7 Ma), and has a short-term presence in NP12 at Avdat, but temporarily disappears, only to re-appear in the NP14a\b transition (47.5 Ma). *Reticulofenestra* group also expresses a diachronous acme, at 52.0 Myr in higher latitudes (Kerguelen plateau, Schneider et al, 2011 and see Fig 1), at ca. 50.0-50.5 Myr in mid-latitude sites DSDP 549 in the North Atlantic, and at Possagno, Italy (Agnini et al, 2006; Galeotti et al, 2019), but only at ca. 47 Myr in the tropic/subtropic Pacific, (ODP Site 1210), and only around 46.0 Myr at Avdat (Fig. 10). Peaks of *Cyclicargolithus luminis* were reported at ca. 51.0 Myr in the Atlantic (ODP site 1263) but at 47.0 in the Pacific ODP Site 1210, as at Avdat. The diachroneity in transition to the *Reticulofenestra / Chiasmolithus* assemblages is a global feature usually dependent on paleolatitude (Haq et al. 1977). Aside from the low latitude position of the Levant margin, the assemblages are strongly affected by proximity to wide and shallow Tethyan shelves of the Afro-Arabia arid belt (Fig. 1). This proximity would maintain warmer waters while open ocean would cool.

388 The sea level axis is subparallel to the oxygen isotope record, as observed in NMDS1 (Fig.
389 7), it is a minor effect reflecting long-term sea level change on the Arabian plate. Until high in NP
390 15-16 (undif.), sea level had hardly any effects on the Avdat section. The position of the section
391 on the outermost portion on the Levant carbonate ramp probably minimized the impact of sea
392 level. Over the long-term, the cooling became a dominant factor. #

393 The warm global ocean of the early Eocene tended to be stratified. That is until the
394 initiation of the cooling trend began when the oceans became destratification and better mixed
395 (Kennett & Stott, 1990). Heat and salinity in the lower latitudes were regulated by a circum-global
396 current flowing across the Tethys from the Late Cretaceous and until possibly the mid-Miocene
397 (Bialik et al, 2019). This current might have been a driver of upwelling systems in the Levant
398 region during the Late Cretaceous. A broad, warm, semi-arid continental margin inhabited the
399 southern margin of Africa. Extensive carbonate platform developed atop this margin, generating a
400 wide shallow water domain, with potential to continue supplying high-salinity bottom and
401 intermediate water.

402 At the P/E boundary the southern Tethys aligned with the global warming trend together
403 with a prominent regional eutrophication and an increase in terrestrial input. Afterwards,
404 Following the P\E boundary the global OBP efficiency began to fall and temperatures increased
405 (Hilting et al, 2008). From NP12, the global warming trend intensified, OBP reached a minimum
406 efficiency and the oceans became stratified and highly oligotrophic. OBP efficiency began to
407 recover in the aftermath of the EECO together with initiation of global cooling and oceanic de-
408 stratification. The oceanic response to the cooling trend began at NP13 (Sloan et al, 1992), and
409 cooling of surface water began in most oceans almost immediately after the peak of the EECO
410 (Schneider et al, 2011). At Avdat, the poor OBP efficiency caused continuation of organic matter
411 accumulation beneath a warm, stratified sea for a further 1 Myr, when compared also with other
412 tropical areas. This delay can be explained by paleogeography of the Levant basin, adjacent to the
413 Afro-Arabian shelf and distant from Tertiary oceanic gyres.

414 **5.3 Temporal variations in the Avdat record**

415 When compared to commonalities of the oceanic sites, the step-out out from the EECO
416 was more eventful in the Levant region than indicated simply by the delay in destratification (Fig.
417 10). The segmentation of the calcareous nannofossil assemblages record shows that intervals of

418 stability are interrupted by short-term perturbations, with the subsequent restored stability evolving
419 over time. This pattern is especially marked in the critical NP14a/b transition period. Following
420 the termination of the EECO at the beginning of NP14a, a short-term shift to *Toweius* dominance
421 restored the calcareous nannofossil assemblage to the well-stratified mode. Further interruptions
422 to stability were characterized by the *Thoracosphaera* and *Braarudosphaera* peaks, co-occurring
423 with decreased preservation quality. Perturbations became less frequent after the NP14b\15
424 boundary, and the DCA analysis (Fig. 9) clearly shows the aberrant trends towards
425 *Thoracosphaera* at Avdat, and their reversal and return to the main ocean trend in the
426 *Reticulosphaera – Chiasmolithus* field. At that time, the pelagic chalk lithofacies becomes more
427 homogeneous, chert and organic-rich horizons become infrequent and gradually disappear in this
428 region. A series of *Thoracosphaera* peaks reappear at Avdat in the upper part of NP 15-16 (undif.).

429 Eocene oscillations expressed by carbon isotope excursions (CIE's), mostly in NP10-NP12,
430 were considered perturbations in sea-water stratification by Galeotti et al. (2019) in Possagno,
431 Italy, on the northern margin of the Mediterranean Tethys. Seven further CIEs were found in NP14
432 (Magnetochron C21r and C21n). These were of smaller magnitude compared to the Eocene
433 Thermal Maximum events in chrons C24n, C24r and C23r. Later on, planktic foraminifera in
434 several low-latitude Indo-Pacific oceanic sites from above middle Eocene calcareous nannofossil
435 zone NP15, also show interruptions of relative stability by cool\warm oscillations of low
436 magnitude superposed upon the global cooling trend (Keller, 1983). These oscillations were
437 attributed there to significant ice accumulation occurring as early as late middle Eocene.

438 In the aftermath of the EECO, the oceanic biological pump efficiency recovered globally.
439 In higher latitudes, assemblages dominated by *Chiasmolithus* spp., indicating the high trophic
440 conditions and elevated nutrients characteristic of mixing in cooler waters. Superficially similar
441 events were recorded in the Avdat section high in NP 15-16 (undif.). These took the form of
442 departure from *Reticulosphaera* assemblage towards *Chiasmolithus* (Fig 10). These features do
443 similarly indicate high trophic conditions and elevated nutrients, but the high-latitude cooling
444 explanation is untenable here. However, specifically in the uppermost part of the section, the
445 eustatic fall in sea level may have finally played a role on the Avdat oceanic environment. Sea
446 level fell, nutrient input from adjacent landmasses sources may have become more significant
447 locally, with *Chiasmolithus* responding accordingly. Later in NP17, Bartonian, Lithofacies in the
448 center of Israel shifts towards marls with terrestrial input (Benjamini, 1980B).

449 The peak in calcareous nannofossil reworking at the base of NP 15-16 (undif.) is for the
450 present unexplained. The mass-transport deposits and perhaps the nummulitic lithofacies in NP 14
451 and late in NP 15-16 (undif.) can be attributed to changes in configuration of the carbonate ramp
452 caused by localized tectonic activity (Buchbinder et al., 1988). Alqudah et al. (2015) assumed that
453 tectonic activity was responsible for multiple peaks in reworking in Jordan. Notably, at Avdat the
454 nummulitic MTD horizons and the reworking peak are not coeval. Collapses driven by ramp
455 steppening would probably have had the fine and coarse fraction supplied together or with a very
456 short lag time. Tectonic movements, and consequent changes in sea floor paleomorphology of the
457 deep ramp margin, may have led to oceanographic changes in current systems, such as
458 reorganization of eddy systems or changes in impingement of contourites. These in turn could
459 affect the scraping mobilization of older fine fraction elements. The aspect of reworking of fine
460 fraction in the region requires further investigation.

461

462

463 ## 6. Conclusions

464 Ecological differences between oceanic sites are generally attributed to paleolatitude, water
465 mass dynamics and changes in temperature gradients. However, land-adjacent oceanic sections as
466 the Levant, on the southern margin of the Tethys, are likely to also encounter influences of climate
467 variability and nutrient input from the boreotropical surrounding (Boucot et al., 2013, Fig. 1).

468 The Avdat calcareous nannofossil assemblages are broadly compliant with the global
469 oceanic trends across the early and middle Eocene. This trend is expressed by shift from *Toweius*
470 dominance to discoasters in the warm early Eocene, followed by shift towards *Reticulofenestra sp*.
471 as cooling took place in the late early and middle Eocene. Sphenoliths -discoasters and *Toweius*
472 dominance are common to both ODP Site 549 and Avdat, terminating in the middle Eocene with
473 *Reticulofenestra* and *Chiasmolithus*.

474 The acme of *Reticulofenestra*, peak *of Chiasmolithus* and the FO of *Cyclocargolithus*
475 *luminis* are delayed by ~1.0 Myr at Avdat with respect to most oceanic sites, and even more so in
476 comparison to higher latitude sites. The southern Tethyan margin appears to have remained
477 stratified long after global mixing has begun in the ocean. This stratification was probably due to

the effect of the warm climate and proximity to even lower latitude saline shelves of the Afro-Arabian margin. Moreover, there is also a delay of nearly 1.5 Myr in the restoration of OBP efficiency at Avdat.

The Avdat section differs from other oceanic sites by interruption of the general trends by short-term events, e.g., of *Blackites* diversity, *Thoracosphaera* peaks, and sporadic presence of *Braarudosphaera*. Most of these events took place from the end NP13 zone to the beginning of NP 15-16 (undif.) across the early/middle Eocene boundary. These events can be attributed to the unique setting of the Avdat section, in the Levant ocean basin sandwiched between the warm, arid Afro-Arabian Tethyan margin to the south, and the active Alpine orogenic belt to the north (*see* Dercourt et al, 1993). During the Paleogene, connectivity of the marine environment to small remnant basins of the Tethys, and back-arc orogenic basins, was intermittent. Contacts between cooler waters sourced in the boreo-tropical belt, and warm, saline low paleo-latitude Tethyan waters, is a special feature the Mediterranean region that is poorly reflected in the open ocean. Neither the Atlantic sites, where there is broad exposure to the boreo-tropical realm and minimal contact with the remainder of the Tethyan shelf, nor in the low-latitude Indo-Pacific realm, where sites at paleolatitudes equivalent to the Tethyan remnants are subject to very different providers of ocean water, exhibit this feature.

Acknowledgments

Parts of this study were carried out in the framework of the Ph.D. thesis of MWH at BGU under supervision of CB. This work was partially supported by an Israeli Ministry of Water and Energy grant number ES-08-16 to CB and Orit Hyams-Kaphzan as well as grants ES-64-2010 and# ES-19-2011. Raw data will be made available through the Pangea.de repository following publication. #

#

:. Reference

Agnini, C., Fornaciari, E., Rio, D., Tateo, F., Backman, J. & Giusberti, L. (2007),

Responses of calcareous nannofossil assemblages, mineralogy and geochemistry to

the environmental perturbations across the Paleocene/Eocene boundary in the Venetian Pre-Alps, *Marine Micropaleontology*, 63, 19–38.

Agnini, C., Muttoni, G., Kent, D. V. & Rio, D. (2006), Eocene biostratigraphy and magnetic stratigraphy from Possagno, Italy: The calcareous nannofossil response to climate variability, *Earth and Planetary Science Letters,* 241, 815– 830.

Alqudah, M., Hussein, M. A., van den Boorn, S., Podlaha, O. G., & Mutterlose, J. (2015), Biostratigraphy and depositional setting of Maastrichtian–Eocene oil shales from Jordan, *Marine and Petroleum Geology*, 60, 87-104.

Ashckenazi-Polivoda, S., Abramovich, S., Almogi-Labin, A., Schneider-Mor, A., Feinstein, S., Püttmann, W. & Berner. Z. (2011), Paleoenvironments of the latest Cretaceous oil shale sequence, Southern Tethys, Israel, as an integral part of the prevailing upwelling system, *Palaeogeography, Palaeoclimatology, Palaeoecology*, 305, 93–108.

Aubry, M.-P., (1986), Paleogene calcareous nannoplankton biostratigraphy of north-western Europe, *Palaeogeography Palaeoclimatology Palaeoecology,* 55, 267-334.

Aubry, M.-P., & Salem, R. (2013), The Dababiya Core: A window into Paleocene to Early Eocene depositional history in Egypt based on coccolith stratigraphy. *Stratigraphy*, 9, 287–346.

Avni, Y. & Weiler, N. (2013), The Geological Map of Israel 1:50,000, Sheet 18-IV: Sede-Boqer. The Geological Survey of Israel, Jerusalem.

Bartov, Y., Reznik, I. & Rozenberg, Y. (2019), Thermal history of the southern Golan basin – geothermal gradient measurements, source rock analysis and basin modelling, Abstracts, Israel Geological Society Annual Meeting, K'far Blum, Israel, p. 19.

Benjamini, C. (1979), Facies relationships of the Avdat Group (Eocene) in the northern Negev, Israel*, Israeli Journal of Earth Science*, 28, 47 - 69.

532 Benjamini, C. (1995), Planktic foraminiferal zonation of the Eocene of Israel, In: *The*
533 *Biostratigraphy of the Eocene in Israel* , edited by H. Schaub, Ch. Benjamini & S.
534 Moshkovitz, Schweizerischen Paläeontologischen Abhandlungen, 117, 33-36.

535 Benjamini, C. (1980), Planktic foraminifera of the 'Avdat Group' (Eocene), *Journal of*
536 *Palaeontology,* 54, 325-358.

537 Benjamini, C. (1980b), Stratigraphy and Foraminifera of the Qezi'ot and Har 'Aqrav Formations
538 (Latest Middle to Late Eocene) of the Western Negev, Israel, *Isr. J. Earth Sci*., 29, 227-
539 244.

540 Bialik, O.M., Frank, M., Betzler, C., Zammit, R. & Waldmann, N.D., (2019), Two-step
541 closure of the Miocene Indian Ocean Gateway to the Mediterranean. *Sci. Rep. 9*,
542 8842. doi:10.1038/s41598-019-45308-7

543 Bison, K-M., Versteegh, G.J.M., Hilgen, F.J. & Willems, H. (2007), Calcareous
544 dinoflagellate turnover in relation to the Messinian salinity crisis in the eastern
545 Mediterranean Pissouri Basin, Cyprus. *Journal of Micropalaeontology,* 26, 103–116.

546 Boucot, A. Xu, C., Scotese, C. & Morley, R.J. (2013), *Phanerozoic Paleoclimate: An Atlas*
547 *of Lithologic Indicators of Climate,* Concepts in Sedimentology and Paleontology,
548 SEPM-Society for Sedimentary Geology.

549 Bown, P. R. & Newsam, C. (2017), Calcareous nannofossils from the Eocene North
550 Atlantic Ocean (IODP Expedition 342 Sites U1403–1411), *Journal of*
551 *Nannoplankton Research,* 37(1), 25-60.

552 Bralower, T. J. (2002), Evidence of surface water oligotrophy during the Paleocene-Eocene
553 thermal maximum: Nannofossil assemblage data from Ocean Drilling Program Site
554 690, Maud Rise, Weddell Sea. *Paleoceanography,* 17, 12-13.

555 Bramlette, N.M. & Sullivan, F.R. (1961), Coccolithophorids and related nannoplankton of
556 the early Tertiary in California, *Micropaleontology,* 7(2), 129-188.

557 Braun, M. (1967), Type sections of Avdat Group Eocene formations in the Negev#
558 (southern Israel), *Stratigraphic Sections*, 4, Geological Survey of Israel.

559 Buchbinder, B., Benjamini, C., Mimran, Y. & Gvirtzman, G. (1988), Mass transport in
560 Eocene pelagic chalk on the north-western edge of the Arabian platform, Shefela
561 area, Israel. *Sedimentology,* 35, 257 - 274.

562 Buzas, M. A. & Hayek, L.A.C. (1998), SHE analysis for biofacies identification. *Journal*
563 *of Foraminiferal Research*, 28(3), 233–239.

564 Clarke, K. R. & Ainsworth, M. (1993), A method of linking multivariate community
565 structure to environmental variables, *Marine Ecology,* 92, 205–219.

566 Clarke, K.R. (1993), Non-parametric multivariate analyses of changes in community
567 structure, *Aust. J. Ecol.,* 18, 117–143.

568 Dercourt, J., Ricou, L. E. & Vrielynck, B. (1993), *Atlas of Tethys palaeoenvironmental maps*, 22
569 maps. in: Atlas of Tethys palaeoenvironmental maps, edited by J. Dercourt, L.E. Ricou &
570 B. Vrielynck, Institut français du pétrole. Bureau d'études industrielles et de coopération,
571 Gauthier-Villars, Paris

572 D'haenens, S., Bornemann, A., Stassen, P. & Speijer, R.P., (2012), Multiple early Eocene
573 benthic foraminiferal assemblage and δ13C fluctuations at DSDP Site 401 (Bay of
574 Biscay — NE Atlantic). *Mar. Micropaleontol.* 88–89, 15–35. doi:
575 10.1016/j.marmicro.2012.02.006

576 de Graciansky P.C., Poag C.W., & Foss. G. (1985), The Deep Sea Drilling Project, Site
577 549- Initial reports, 80 U.S. Government printing office,
578 doi:10.2973/dsdp.proc.80.101.

579 Ehrlich, A. & Moshkovitz, S. (1982), Paleogene calcareous nannofossil biozonation in
580 Israel. Geological Survey of Israel, Jerusalem. *Current Research*-1981, 35 – 41

581 Eshet, Y., Moshkovitz, S., Habib, D., Benjamini, C. & Magaritz, M. (1992), Calcareous
582 nannofossil and dinoflagellate stratigraphy across the Cretaceous Tertiary boundary
583 at Hor Hahar, Israel, *Marine Micropaleontology,* 18, 199-228.

584 Fermont, W. J. J. (1982), *Discocyclinidae* from Ein Avdat (Israel). *Utrecht*
585 *Micropaleontological Bulletins,* 4, 152p.

586 Galeotti, S., Sprovieri, M., Rio, D., Moretti, M., Francescone, F., Sabatino, N., Fornaciari,
587 E., Giusberti, L. & Lancia, L. (2019), Stratigraphy of early to middle Eocene
588 hyperthermals from Possagno (Southern Alps, Italy) and comparison with global
589 carbon isotope records, *Palaeogeography, Palaeoclimatology, Palaeoecology*, 527,
590 39-52. https://doi.org/10.1016/j.palaeo.2019.04.027#

591 Gangyi, L., Keller, G., Adatte, T. & Benjamini, C. (1995), Abrupt change in the upwelling
592 system along the southern margin of the Tethys during the Paleocene-Eocene
593 transition event, *Isr. Jour. Earth Sci.,* 44, 185-197.

594 Haq, B.U., Premoli-Silva, I. & Lohmann, G.P. (1977), Calcareous plankton
595 paleobiogeographic evidence for major climatic fluctuations in the early Cenozoic
596 Atlantic Ocean. *J. Geophys. Res*, 82, 3861–3876. doi:10.1029/JC082i027p03861

597 Haq, B. U. & Al-Qahtani, A. M. (2005), Phanerozoic cycles of sea-level change on the
598 Arabian Platform Rationale for an Arabian Platform Cycle Chart, *GeoArabia* 10,
599 127–160.

600 Hilting, A.K., Kump, L.R. & Bralower, T.J. (2008), Variations in the oceanic vertical
601 carbon isotope gradient and their implications for the Paleocene–Eocene biological
602 pump, *Paleoceanography*, 23 (PA3222).

603 Keller, G. (1983), Paleoclimatic analyses of middle Eocene through Oligocene planktic
604 foraminiferal fauna, *Palaeogeography, Palaeoclimatology, Palaeoecology,* 43, 73-
605 94.

606 Kennett, J.P. & Stott, L.D. (1990), Proteus and Proto-Oceanus: Ancestral Paleogene oceans
607 as revealed from Antarctic stable isotopic results, *Proc. Ocean Drill, Program Sci.*
608 *Results,* 113, 865–880.

609 Kohn, M. & Zonneveld., K. A.F. (2010), Calcification depth and spatial distribution of
610 *Thoracosphaera heimii* cysts: Implications for palaeoceanographic reconstructions,
611 *Deep-Sea Research,* I57, 1543–1560

612 Martini, E. (1971), Standard Tertiary and Quaternary calcareous nannoplankton zonation,
613 In: *Proceedings of the Second Plank tonic Conference, Roma*. edited by A.
614 Farrinacci, Edizioni Tecnoscienza, Rome, p. 739 - 785#

McArthur, J.M., Howarth, R.J. & Shields, G.A. (2012), Strontium Isotope Stratigraphy. In *The Geologic Time Scale 2012* edited by F.M. Gradstein, J.G. Ogg, M.D. Schmitz, and G.M. Ogg, Volume 2, Elsevier BV. doi: 10.1016/B978-0-444-59425-9.00001-9

Meilijson, A. Bialik, O.M., Coletti, G., Waldman, N., Benjamini, C, Sepulveda, J. & Makovsky, Y. (2019), A regional investigation of an under-considered source rock in the Eastern Mediterranean: organic rich carbonates from the Eocene of the Levant margins, Abstract, AAPG-Geoscience Technology Workshop, Tel Aviv, Israel.

Meilijson, A., Ashckenazi-Polivoda, S., Ron-Yankovich, L., Illner, P., Alsenz, H., Speijer, R. P. & Abramovich, S. (2014), Chronostratigraphy of the Upper Cretaceous high productivity sequence of the southern Tethys, Israel. *Cretaceous Research*, 50, 187-213.

Moshkovitz, S. (1995), Calcareous nannofossils from the Lower Tertiary nummmulitic beds of the Negev. In *The Biostratigraphy of the Eocene in Israel,* edited by H. Schaub, Ch. Benjamini, and S. Moshkovitz, Schweizerischen Paläeontologischen Abhandlungen, 117, 41-46.

Muller, C. (1985), Biostratigraphic and paleoenvironmental interpretation of the Goban Spur region based on a study of calcareous nannoplankton. In *The Deep Sea Drilling Project* edited by P.C. de Graciansky, C.W. Poag and G. Foss, *Site 549- Initial reports,* 80, U.S. Government printing office.

Nielsen, S.G., Mar-Gerrison, S., Gannoun, A., LaRowe, D., Klemm, V., Halliday, A.N., Burton, K.W. & Hein, J.R., (2009), Thallium isotope evidence for a permanent increase in marine organic carbon export in the early Eocene. *Earth Planet. Sci. Lett*, 278, 297–307. doi: 10.1016/j.epsl.2008.12.010

Okada, H. & Bukry, D. (1980), Supplementary modification and introduction of code numbers to the low-latitude coccoliths biostratigraphic zonation (Bukry, 1973; 1975), *Marine Micropaleontology*, 5, 321-325.

Ozdinova, S. (2013), Paleoecological evaluation of calcareous nannofossils from the Eocene and Oligocene sediments of the Subarctic Group of the Western Carpathians, *Mineral. Slov.,* 45, 1-10.

Perch-Nielsen, K. (1985), Mesozoic calcareous nannofossils. In: *Plankton Stratigraphy*, edited by H.M. Bolli, J.B. Saunders, and K. Perch - Nielsen, Cambridge University Press, Cambridge, pp. 329 - 426

Romein, A. J. T. (1979), Lineages in early Paleogene calcareous nannoplankton, *Utrecht Micropaleontological Bulletin,* 22, 231pp.

Schaub, H., (1995), Nummulites of Israel. In: *The Biostratigraphy of the Eocene in Israel*, edited by H. Schaub, Ch. Benjamini, & S. Moshkovitz, Schweizerischen Paläeontologischen Abhandlungen, 117, part II, 19-32.

Scheibner, C. & Speijer, R.P. (2008), Late Paleocene–early Eocene Tethyan carbonate platform evolution, A response to long- and short-term paleoclimatic change, *Earth-Science Reviews,* 90, 71–102.

Schmitz, B., Charisi, S. D., Thompson, E. I. & Speijer, R. P. (1997), Barium, SiO_2 (excess), and P_2O_5 as proxies of biological productivity in the Middle East during the Palaeocene and the latest Palaeocene benthic extinction event. *Terra Nova,* 9, 95–99.

Schmitz, M.D. (2012), Appendix A: Radiometric ages used in *The Geologic Time Scale 2012*, edited by F.M. Gradstein, J.G. Ogg, M.D. Schmitz & G.M. Ogg, Volume 2, Elsevier BV. doi: 10.1016/B978-0-444-59425-9.00001-9

Schneider, L.J., Bralower, T.J. & Kump, L.R. (2011), Response of nannoplankton to early Eocene ocean destratification, *Palaeogeography, Palaeoclimatology, Palaeoecology,* 310, 152–162.

Shafik, S. (1989), Some new calcareous nannofossils from Upper Eocene and Lower Oligocene sediments in the Otway Basin, southeastern Australia. *Alcheringia,* 13, 69-83.

Sloan L.C, Walker, J.C.G., Moore Jr., T.C. Rea, D.K. & Zachos, J.C. (1992), Possible methane-induced polar warming in the early Eocene, *Nature,* 357, 320-322.

Somerfield, P.J., Clarke, K.R. & Warwick, R.M. (2008), Simpson index. In: *Encyclopedia of Ecology,* edited by S.V. Jorgensen and B. Fath, Elsevier, Oxford, UK, pp. 3252-3255.

672 Speijer, R. P. (1995), The late Paleocene benthic foraminiferal extinction as observed in
673 the Middle East. In : *Paleocene-Eocene boundary events; proceedings of the co-*
674 *ordinators meeting,* edited by P. Laga, Bulletin de la Societe Belge de Geologie,
675 Bulletin van de Belgische Vereniging voor Geologie, 103, 267-280.

676 Tantawy, A. (2003), Calcareous nannofossil biostratigraphy and paleoecology of the
677 Cretaceous–Tertiary transition in the central eastern desert of Egypt, *Marine*
678 *Micropaleontology*, 47, 323–356.

679 Tori, F. & Monechi, S. (2013), Lutetian calcareous nannofossil events in the Agost section
680 (Spain): Implications toward a revision of the middle Eocene
681 biomagnetostratigraphy, *Lethaia,* 46, 293-307, doi: 10.1111/let.12008

682 Tremolada, F. & Bralower, T.J. (2004), Nannofossil assemblage fluctuations during the
683 Paleocene– Eocene Thermal Maximum at Sites 213 (Indian Ocean) and 401 (North
684 Atlantic Ocean): Palaeoceanographic implications, *Marine Micropaleontology*, 52,
685 107–116.

686 Weinbaum Hefetz, M. & Bartov, Y. (2019), High resolution calcareous nannofossil
687 chronology of the Eocene sequence in the southern Golan basin. Abstracts, Israel
688 Geological Society Annual Meeting, K'far Blum, Israel, p. 127.

689 Weinbaum-Hefetz, M. & Benjamini, C. (2011), Calcareous nannofossil assemblage
690 changes from early to middle Eocene in the Levant margin of the Tethys, central
691 Israel, *Jour. of Micropalaeontology*, 30, 129–139.

692 Weinbaum-Hefetz, M., Benjamini, C. & Moshkovitz, S. (2000), Genus *Rhabdosphaera*
693 Haeckel across the lower/middle Eocene boundary at the Avdat Plateau in Israel:
694 Biostratigraphy and possible paleoeoecological interpretation*. In: Early Paleogene*
695 *warm climates and biosphere dynamics,* short papers and extended abstracts, edited
696 by B. Schmitz, B. Sundquist & F.P. Andreasson, GFF, 122,176- 177.

697 Young, J. R., Bergen, J. A., Bown, P. R., Burnett, J. A., Fiorentino, A., Jordan, R. W.,
698 Kleijne, A., van Niel, B.E., Romein, A. J. T. & von-Salis, K. (1997), Guidelines for
699 coccolith and calcareous nannofossil terminology. *Palaeontology,* 40, 875-912

Young, J. R. & Bown, P. R. (1997), Cenozoic calcareous nannoplankton classification, *Journal of Nannoplankton Research,* 19, 36-47.

Young, J. R. & Ziveri, P. (2000), Calculation of coccolith volume and its use in calibration of carbonate flux estimates, *Deep Sea Research Part II: Topical Studies in Oceanography,* 47, 1679-1700.

Zachos, J., Pagani, M., Sloan, L., Thomas, E. & Billups, K. (2001), Trends, rhythms, and aberrations in global climate 65 Ma to present, *Science,* 292, 686–693.

Zachos, J.C., Kroon, D. & Blum, P. (2004), SITE 1263- Shipboard Scientific Party. Proceedings of the Ocean Drilling Program, Initial Reports Volume 208.

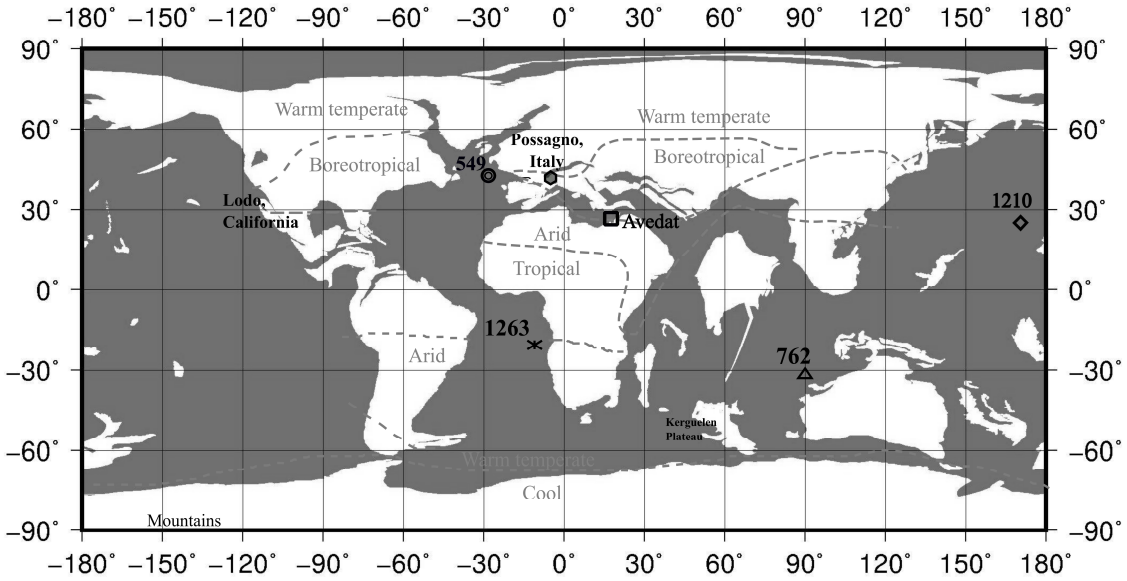

Figure 1. Selected sites on a paleogeographic reconstruction of the Eocene (51Ma). Location of Avdat (Israel), Possagno (Italy), Lodo Formation (California), the Keguelen plateau, and the DSDP\ODP sites are shown. Source for continental reconstruction is the Ocean Drilling Stratigraphic network (www.odsn.de). Paleoclimate belts redrawn following Boucot et al. (2013). Symbols for sites in this study are consistent in all figures.

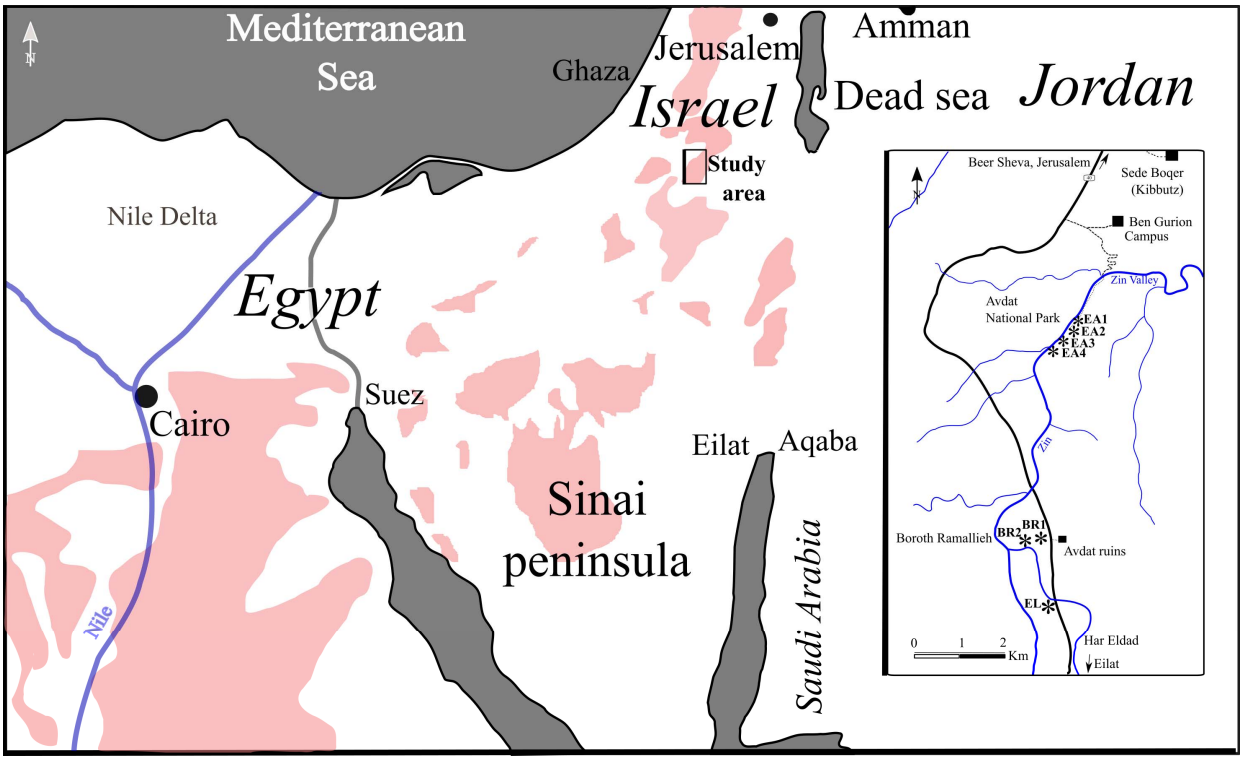

Figure 2. Eocene outcrops in the southern Levant and location of Avdat sections. a. Eocene outcrops in Egypt and Israel shown in color; b. Seven subsections along Zin Valley near Avdat (EA1, EA2, EA3, EA4, BR1, BR2 and EL) were used for the current study, comprising the NP11 to NP15-16 (undiff.) interval.

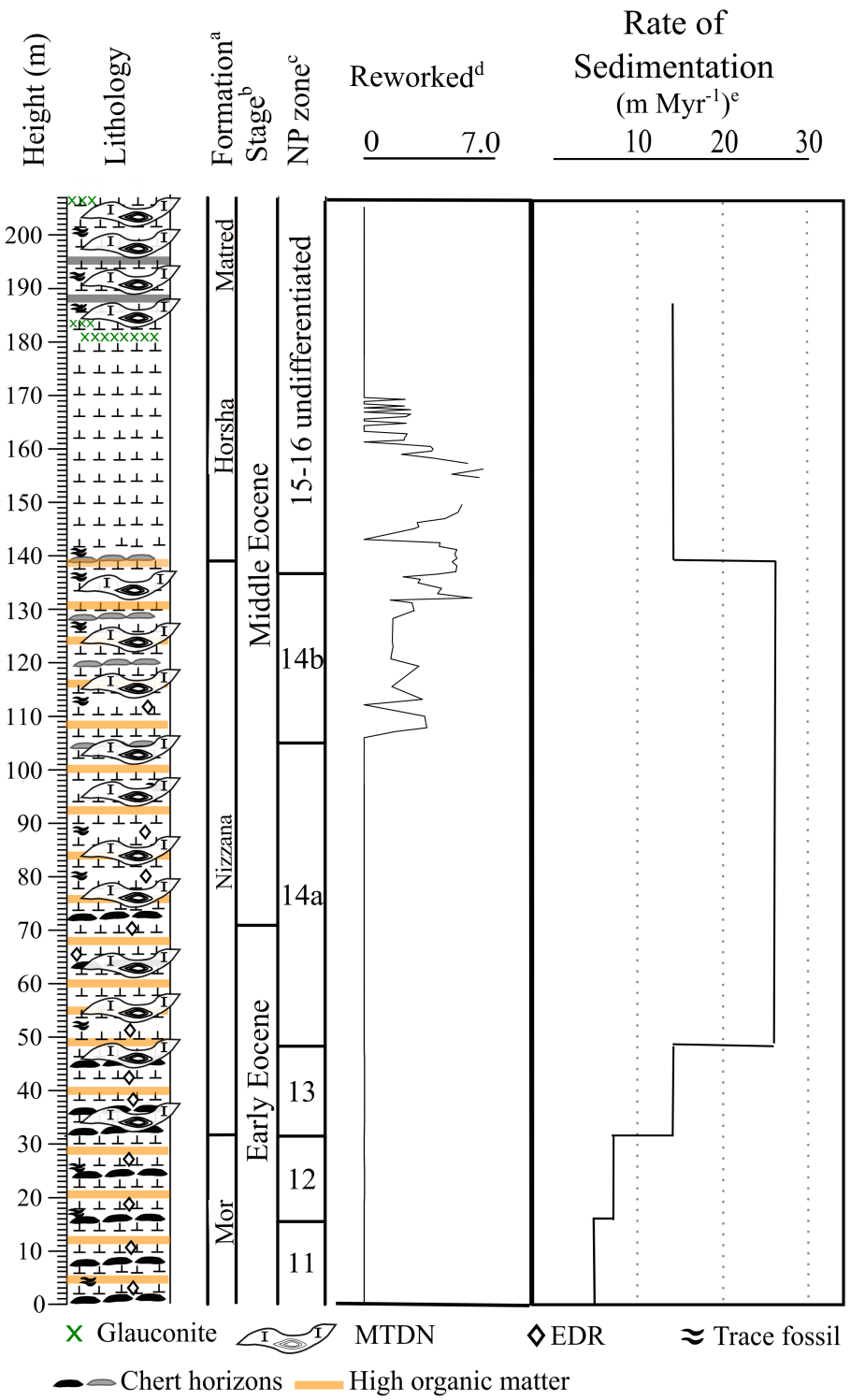

Figure 3. Integrated columnar section of the Avdat Eocene outcrops. a. Lithological units after map of Avni & Weiler (2013); b. The Early \Middle Eocene boundary following GTS2012; c. NP zones (Weinbaum Hefetz & Benjamini, 2011, following Martini, 1971); d. Percent reworked species (Weinbaum Hefetz & Benjamini, 2011); e. Rates of sedimentation (NP11 recalculated after Romein, 1979). MTDN - mass transport deposits with Nummulites, EDR – euhedral dolomite rhombs.

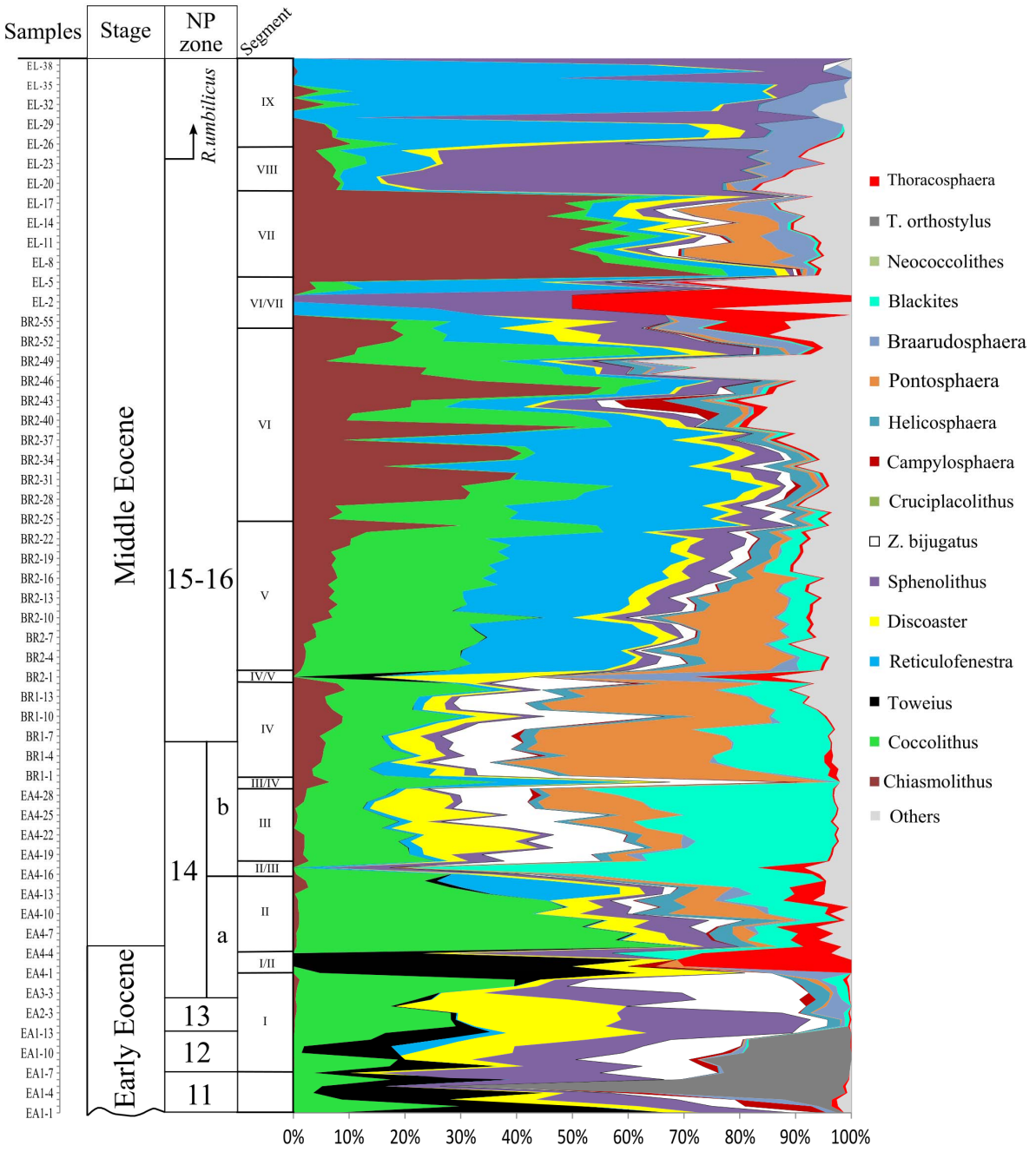

732

733 **Figure 4**. Cumulative-% area representation of the major groups of calcareous nannofossils in the Avdat section.
734 Sample numbers shown against NP zones of Martini (1971).

735

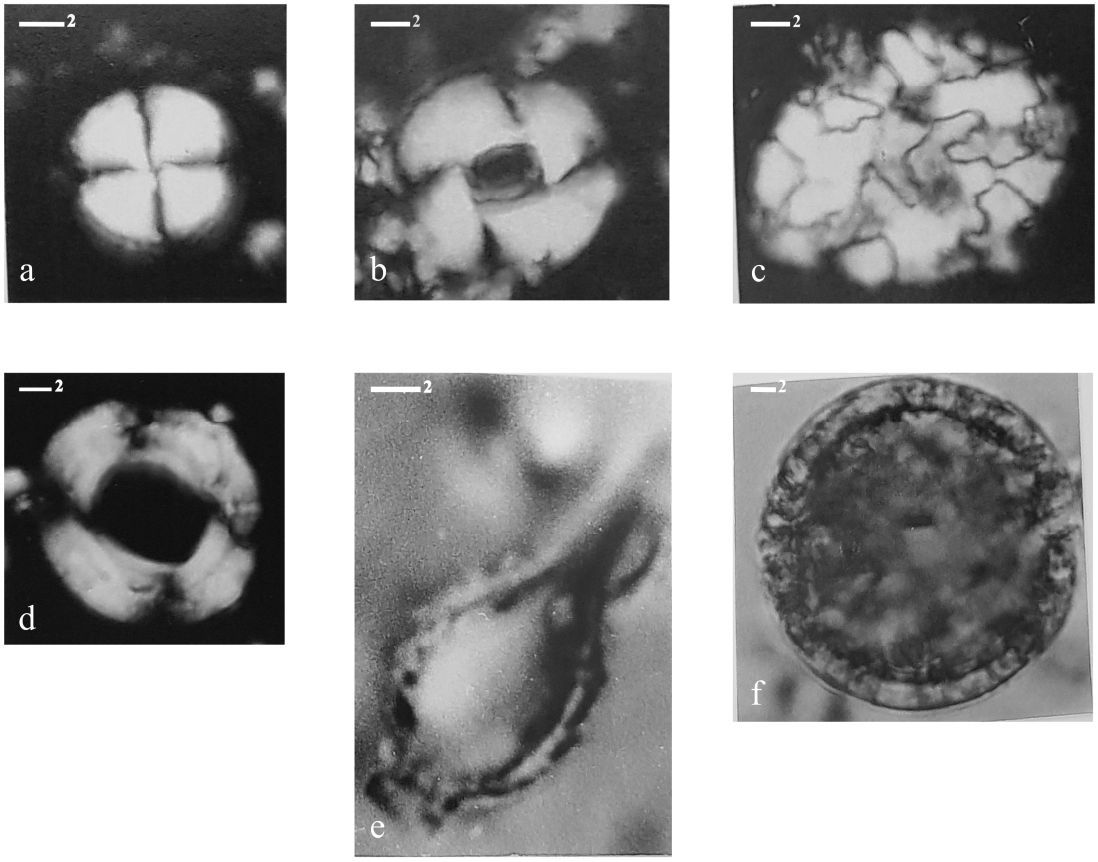

Figure 5. Photomicrographs of selected calcareous nannofossils in the Avdat section. Scale in micrometers. a. *Cyclicargolithus luminis*, crossed-nicols, BR2 -55.; b. *Reticulofenestra dictyoda*, crossed-nicols, BR1-2; c. *Thoracosphaera heimii*, crossed- nicols, BR2-55; d. *Reticulofenestra umbilicus*, crossed-nicols, EL-25; e. *Blackites piriformis*, PPL, EA4-17; f. *Thoracosphaera* sp., PPL, BR2-45. (Original film photography by MWH*1)

742

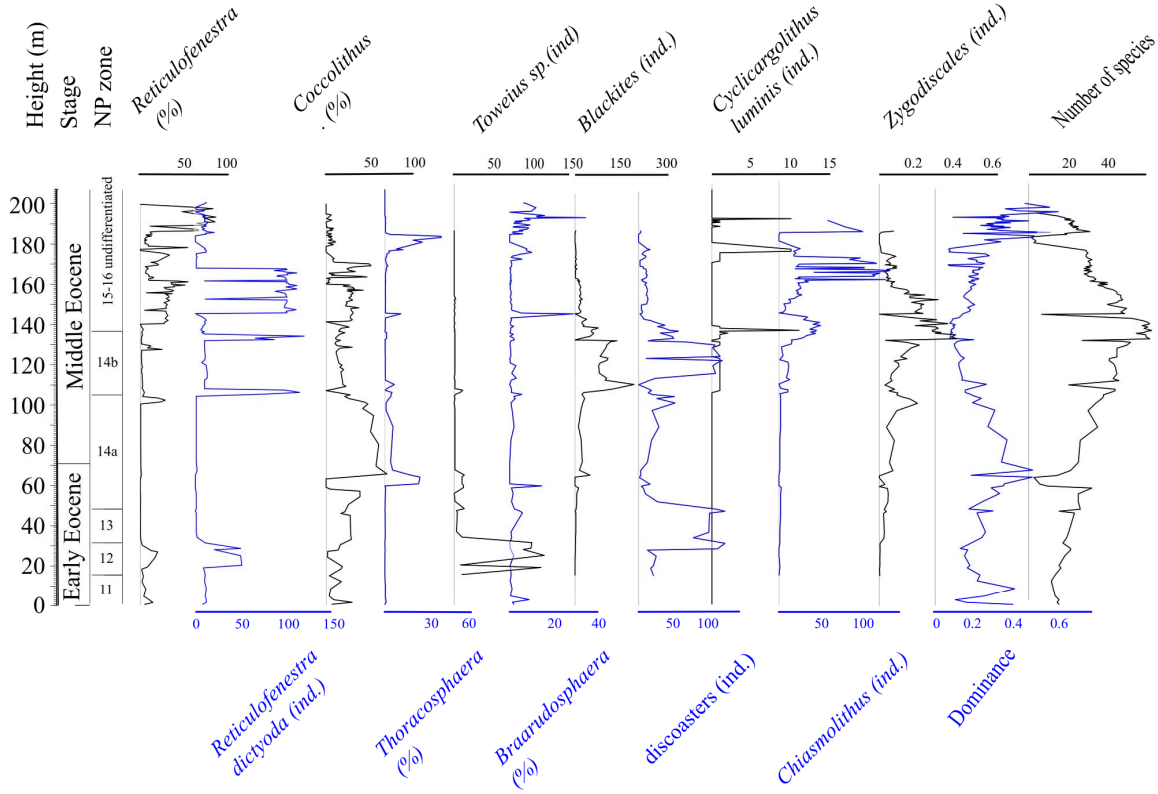

743

744 **Figure 6**. Count profiles in the Avdat section. Selected calcareous nannofossil groups used as biotic variables, counts
745 (ind.) or %, number of species (Richness) and Dominance (Simpson's index of dominance).

746

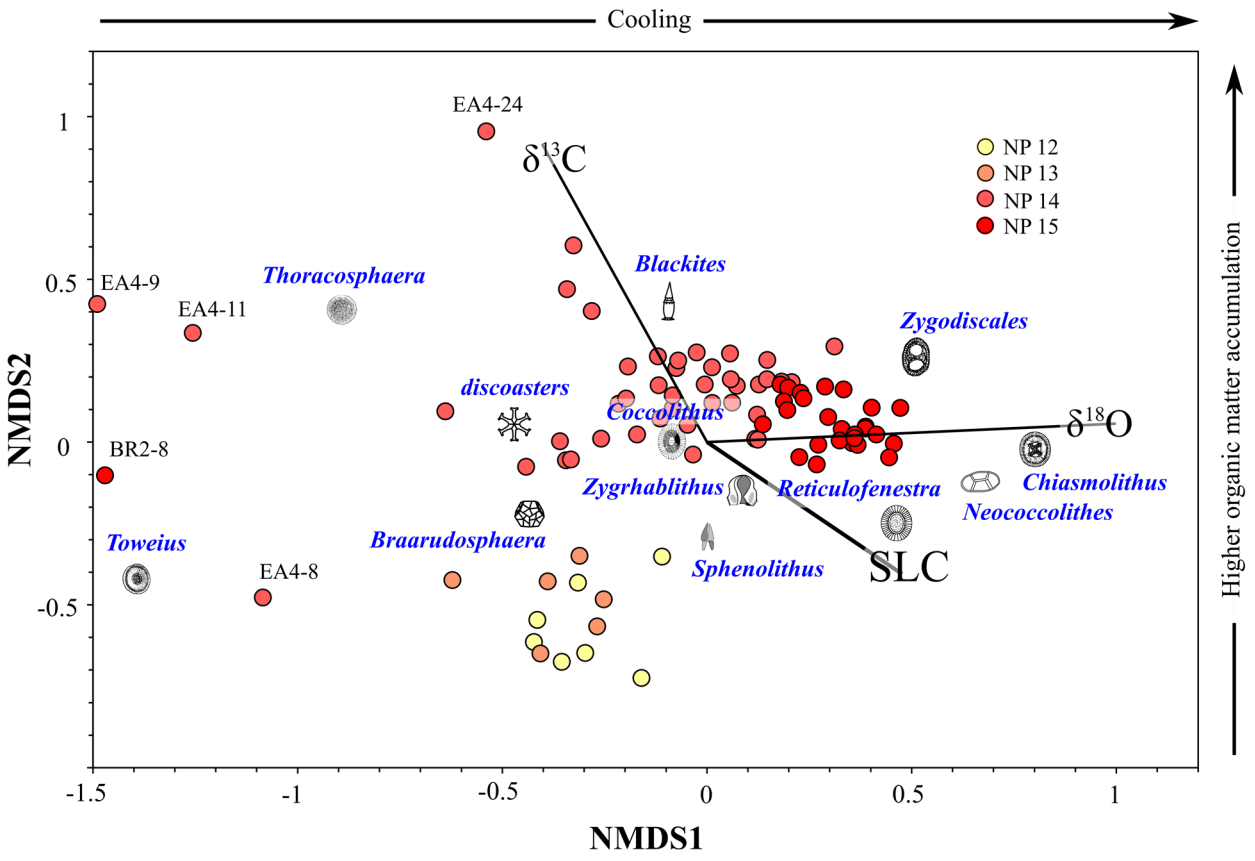

747

748 **Figure 7**. Projection of ENVFIT on selected calcareous nannofossil groups of the Avdat section. NP zones are marked
749 from yellow to red. Calcareous nannofossil group fields are in blue. ENVFIT vectors are based on C and O stable
750 isotope data of Zachos et al (2001) and Arabian plate sea level changes (SLC) of Haq & Al-Qahtani (2005). 2D stress
751 = 0.14 including outliers.

752

753

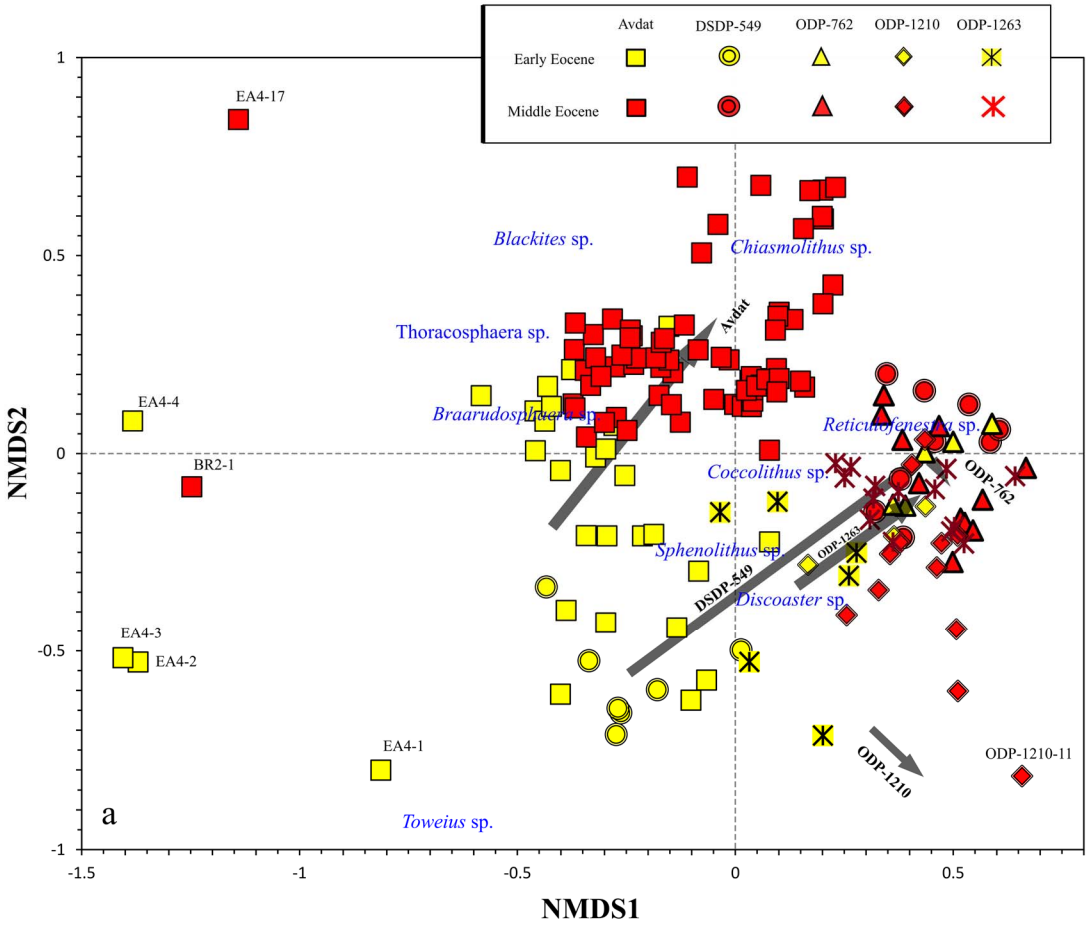

754

755 **Figure 8**. NMDS Projection of the calcareous nannofossil assemblages in DSDP/ODP sites compared to Avdat. NP
756 zones are marked from yellow to red and calcareous nannofossil group fields in blue as in Fig. 7. Note outlier samples.
757 Grey arrow size and direction indicate the shift of the early to middle Eocene centroids. 2D stress = 0.19.

758

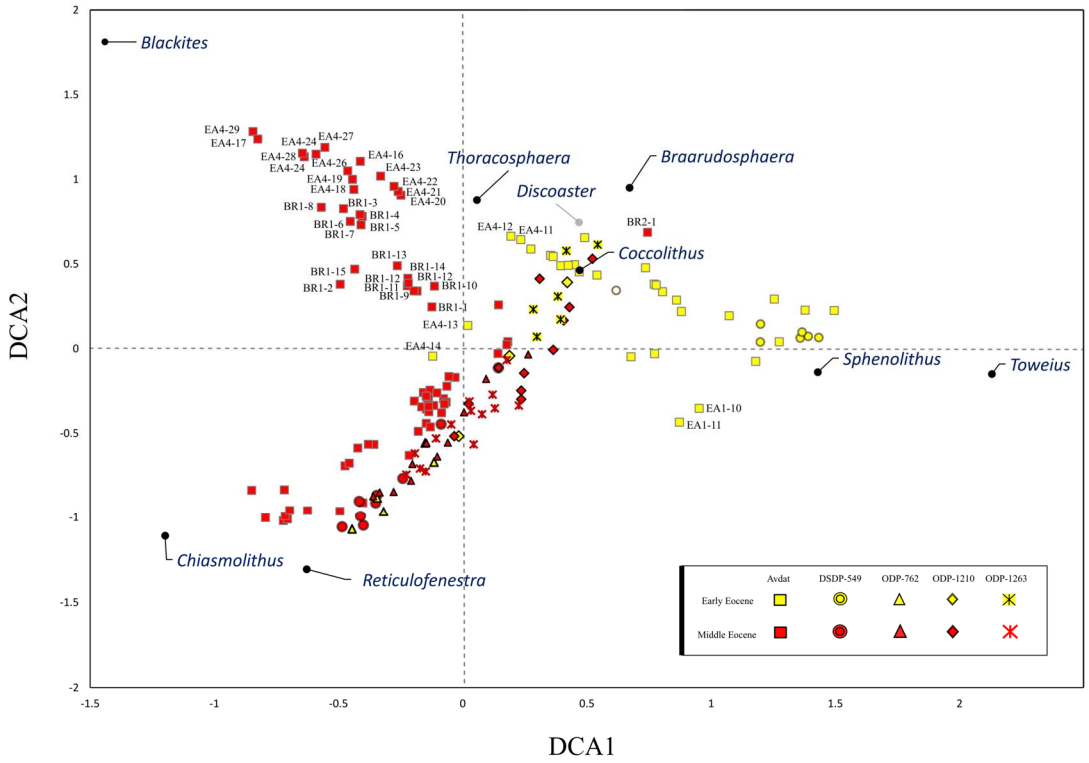

759

760 **Figure 9**. Detrended Correspondence Analysis (DCA) of the DSDP/ODP data compared to the Avdat section. NP
761 zones are marked from yellow to red and calcareous nannofossil group fields in blue as in Fig. 7. Note outlier fields
762 of Avdat. Eigenvalues: DCA1=0.33, DCA2= 0.36. DCA3 and DCA4 values are both 0.17.

763

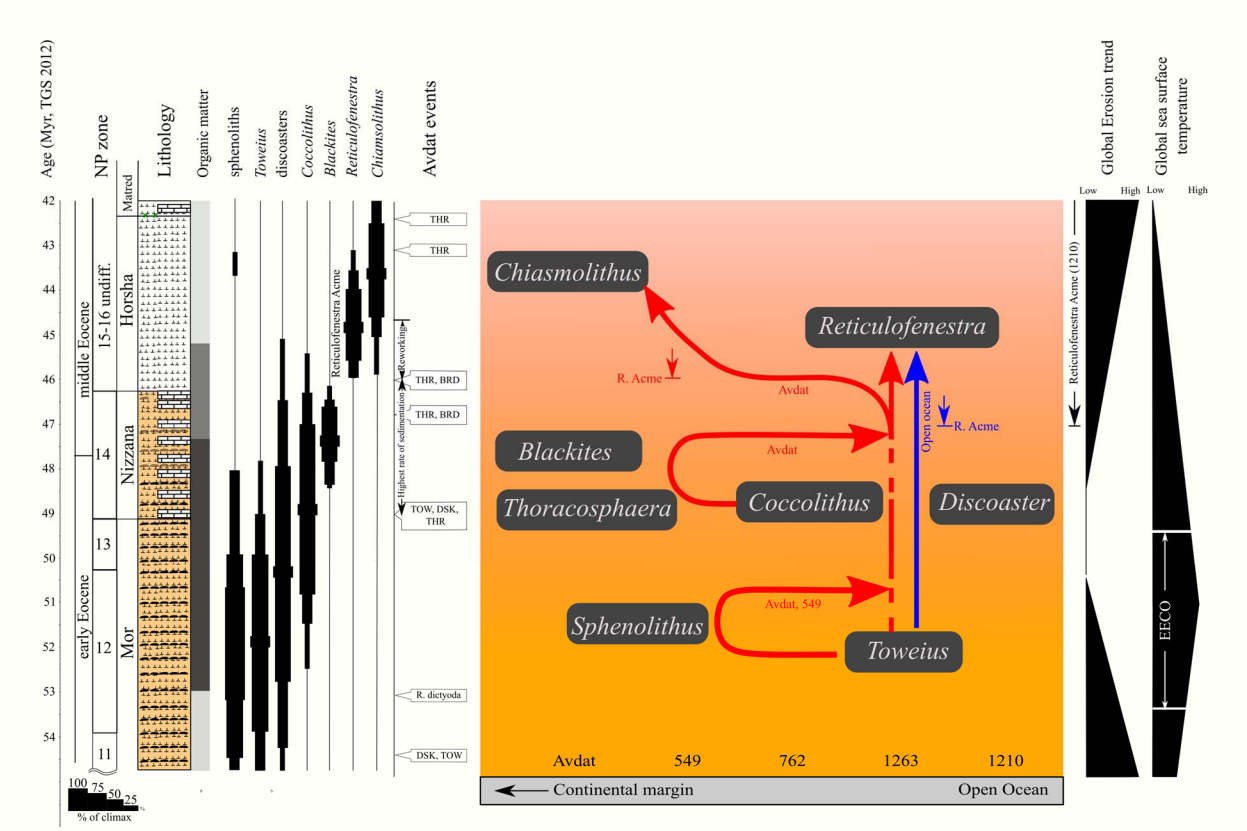

764

765 **Figure 10**. Compilation of sequence of events at Avdat compared to oceanic sites. Trends in global ocean shown in
766 blue, departures at Avdat in red, and delay in Reticulofenestra acme at Avdat marked. Organic matter-rich parts at
767 Avdat shown by darker color. Relative abundances of major groups are % of maximum values. Position of short-term
768 events (STE) in early\middle Eocene transition placed in respect to GTS 2012 age model; DSK – discoasters; TOW –
769 Toweius; THR – Thoracosphaera; BRD – Braarudosphaera. Schematic global erosion rates and sea surface
770 temperatures based on published isotope data (see text for references).

771